Photon Energy Deposition in Strong-Field Single Ionization of Multielectron Molecules

Wenbin Zhang,[1] Zhichao Li,[2] Peifen Lu,[1] Xiaochun Gong,[1] Qiying Song,[1] Qinying Ji,[1] Kang Lin,[1] Junyang Ma,[1] Feng He,[2,*] Heping Zeng,[1,†] and Jian Wu[1,3,‡]

[1]*State Key Laboratory of Precision Spectroscopy, East China Normal University, Shanghai 200062, China*
[2]*Key Laboratory of Laser Plasmas (Ministry of Education) and Department of Physics and Astronomy, Collaborative Innovation Center for IFSA (CICIFSA), Shanghai Jiao Tong University, Shanghai 200240, China*
[3]*Collaborative Innovation Center of Extreme Optics, Shanxi University, Taiyuan, Shanxi 030006, China*

(Received 9 April 2016; published 1 September 2016)

Molecules exposed to strong laser fields may coherently absorb multiple photons and deposit the energy into electrons and nuclei, triggering the succeeding dynamics as the primary stage of the light-molecule interaction. We experimentally explore the electron-nuclear sharing of the absorbed photon energy in above-threshold multiphoton single ionization of multielectron molecules. Using CO as a prototype, vibrational and orbital resolved electron-nuclear sharing of the photon energy is observed. Different from the simplest one- or two-electron systems, the participation of the multiple orbitals and the coupling of various electronic states in the strong-field ionization and dissociation processes alter the photon energy deposition dynamics of the multielectron molecule. The population of numerous vibrational states of the molecular cation as the energy reservoir in the ionization process plays an important role in photon energy sharing between the emitted electron and the nuclear fragments.

DOI: 10.1103/PhysRevLett.117.103002

Many interesting phenomena have been observed for molecules exposed to strong laser fields, e.g., the bond softening and hardening [1–4], above-threshold dissociation [5,6], tunneling dissociation [7], Coulomb explosion [8–10], charge-resonance-enhanced ionization [11,12], and high harmonic generation [13–15]. Differing from single-photon ionization induced by synchrotron radiation [16–18], atoms and molecules may coherently absorb multiple photons beyond the minimal number required for ionization driven by a strong laser field, leading to discrete energy peaks in the photoelectron spectrum spaced by the photon energy, i.e., above-threshold ionization as first observed by P. Agostini *et al.* in 1979 [19]. The primary stage of light-molecule interaction is the photon energy absorption and deposition. As compared to atoms where the electron keeps most of the absorbed photon energy, the additional vibrational and rotational nuclear motions of molecules also serve as energy reservoirs. The photon energy deposited into the nuclei governs the succeeding dynamics and thus the fate of the molecule.

Until recently, the electron-nuclear sharing of the absorbed photon energy in strong-field multiphoton single ionization of molecules was revealed for the simplest one- or two-electron systems of H_2^+ [20–27] and H_2 [28]. On the other hand, the recent experiments showed negligible photon energy sharing between the emitted electrons and ions in double ionization of a polyatomic hydrocarbon molecule [29]. Does the electron-nuclear sharing of the absorbed photon energy in multiphoton ionization of molecules merely exist in the simplest one- or two-electron systems of H_2^+ and H_2? Which rules govern the electron-nuclear sharing of the absorbed photon energy? Understanding the multiphoton energy sharing between the electrons and nuclei provides deep insight into the strong-field dynamics of multielectron molecules where multiple orbitals and numerous electronic states are entangled in the ionization and dissociation processes.

In this Letter, we demonstrate experimental observation of the electron-nuclear sharing of the absorbed photon energy in strong-field above-threshold dissociative single ionization of multielectron molecules. Vibrational and orbital resolved electron-nuclear sharing of the absorbed photon energy is identified for the CO molecule. Depending on the detailed electronic and nuclear structures of the molecule, the photon energy sharing between the electron and nuclei is dominated by the population of numerous vibrational states of the ionization created molecular cation. As compared to the one- or two-electron systems, the observed electron-nuclear photon energy deposition dynamics of the multielectron molecule are altered by the molecular orbitals from which the electron is extracted and the potential energy surfaces of the electronic state on which the nuclei dissociate.

Experimentally, we performed the measurements in an ultrahigh vacuum reaction microscope of cold target recoil ion momentum spectroscopy [30,31], where the laser ionization created ions and electrons were detected in coincidence by two time- and position-sensitive micro-channel plate detectors [32] at the opposite ends of the spectrometer. The three-dimensional momenta vectors of the detected ions and electrons were retrieved from the measured times of flight and positions of the impacts during the offline analysis. To get a well-spaced above-threshold ionization spectrum of the emitted photoelectron in the

multiphoton ionization regime, a linearly polarized ultraviolet (UV) femtosecond pulse centered at 395 nm was produced by frequency doubling a near-infrared pulse from a multipass amplifier Ti:sapphire laser system (25 fs, 790 nm, 10 kHz) in a 150-μm-thick β-barium borate crystal. The laser pulses were tightly focused onto a supersonic molecular beam of CO by using a concave silver mirror ($f = 7.5$ cm) inside the vacuum chamber. By tracing the field-intensity-dependent shift of the sum energy of electron and nuclei from dissociative single ionization of H_2 [33], the laser field intensity of the UV pulse in the interaction region was estimated to be 7.6×10^{13} W/cm^2 with a temporal duration of $\sim 70 \pm 3$ fs. The corresponding Keldysh parameter was calculated to be $\gamma = 2.48$.

To reveal the photon energy sharing between the electron and nuclei, we focus on the dissociative single ionization channel, i.e., $CO + qh\omega \rightarrow C^+ + O + e$ labeled as $CO(1,0)$, by using the electron-nuclear joint energy spectrum (JES), i.e., E_e vs E_N [31]. The kinetic energy of the neutral fragment (not detected directly) is calculated according to the recoil momentum of the fragment ion and electron ejected from the same molecule and included in the total kinetic energy of the nuclei E_N.

Figure 1(a) displays the measured electron-nuclear JES of the $CO(1,0)$ channel driven by a linearly polarized 395-nm pulse. The corresponding energy spectrum of the nuclei E_N integrated over E_e is displayed in Fig. 1(b).

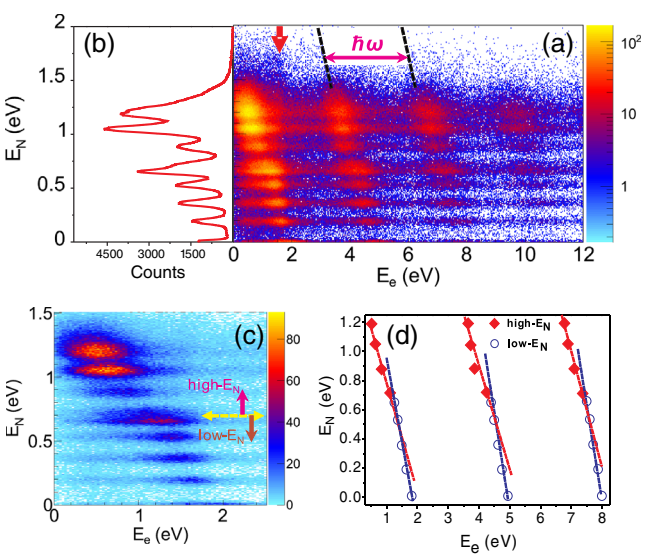

FIG. 1. (a) Measured electron-nuclear JES of the $CO(1,0)$ channel in a linearly polarized 395-nm femtosecond laser pulse. (b) The corresponding nuclear spectrum E_N integrated over E_e. (c) Enlarged JES distribution of the first diagonal line in (a). Two JES structures are identified as separated by a dashed yellow arrow at $E_N \sim 0.7$ eV, referred to as the low- and high-E_N regions. (d) Distribution of the energy peaks of the discrete islands in the first three JES diagonal lines in (a). Two distinct JES structures in the low- and high-E_N regions show different photon energy sharing slopes.

Differing from the multiphoton double ionization of polyatomic acetylene [29], as shown in Fig. 1(a), multiple diagonal lines spaced by the photon energy of the driven laser field are observed in the electron-nuclear JES of the $CO(1,0)$ channel, indicating the photon energy sharing between the emitted electron and nuclei in strong-field ionization of a multielectron molecule. The excess photon energy over the ionization threshold is not only deposited to the outgoing electron, but also transferred to the heavy nuclei via their correlated interactions. As compared to the $H_2{}^+$ [20–27] or H_2 [28], the light may directly interact with the nuclei for the heteronuclear diatomic molecule having a permanent dipole. However, for CO the dipole moments of the nuclei and the three highest occupied molecular orbitals (HOMOs) are estimated to be 0.0028 (nuclei), 0.4486 (HOMO), 0.2909 (HOMO-1), and 0.3232 Debye (HOMO-2), respectively. Although we cannot experimentally distinguish their contributions to the observed E_N, the direct dipole coupling of the light with the nuclei is 2 orders of magnitude smaller than that of the electron. The electron-nuclear photon energy sharing is mainly via the electron-nuclei coupling.

Interestingly, the JES reveals much more than the energy sharing features. As shown in Fig. 1(a), the diagonal lines in the electron-nuclear JES of the $CO(1,0)$ channel show discrete fine structures in E_N, which maps the rich vibrational structure of the multiphoton ionization created molecular cation. The strong-field multiphoton dissociative single ionization of the molecule can generally be understood as a two-step process. The molecule emits one electron and populates various vibrational states of the molecular cation by absorbing multiple photons in the ionization step. The created vibrational nuclear wave packet afterwards dissociates into a neutral and an ionic fragment assisted by photon-coupled transitions among various potential energy curves. As displayed in Fig. 1(a), it shows discrete fine energy structures in each individual diagonal line of the electron-nuclear JES by mapping the vibrational states of the intermediate states populated in the ionization process.

For multielectron molecules, multiple orbitals and electronic states [34,35] are coupled by the strong laser fields in the ionization and dissociation processes, which are encoded in the observed electron-nuclear JES. Figure 1(c) shows the enlarged distribution of the first diagonal line of the JES where two sets of electron-nuclear energy sharing structures coexist and are distinguished as the low-E_N and high-E_N regions, respectively, for E_N larger or smaller than 0.7 eV. The intensity of the JES distribution increases with increasing nuclear energy for each JES set. As shown in Fig. 1(d), the peak energies of the discrete islands in the first three diagonal lines of the JES show different slopes for the low ($s_{1st} = -1.14 \pm 0.03$, $s_{2nd} = -1.19 \pm 0.05$, $s_{3rd} = -1.30 \pm 0.05$) and high ($s_{1st} = -0.77 \pm 0.07$, $s_{2nd} = -0.73 \pm 0.18$, $s_{3rd} = -0.79 \pm 0.08$) E_N regions, indicating distinct photon energy deposition dynamics. It was demonstrated that the interplay of the inter- and

intracycle interferences of the released electron in the strong-field ionization of $H_2{}^+$ affects the slope of the resulting electron-nuclear JES structure [27]. As we will discuss below, for CO these two distinct JES structures also correlate with the electron releasing from different orbitals and photon-assisted coupling of various electronic states in the ionization and dissociation processes.

Figure 2(a) shows the relevant potential energy curves of the CO and CO^+ calculated using the molpro [36] with the multireference configuration interaction method based on the augmented correlation consistent polarized valance quadruple zeta basis set [37]. Removal of an electron from the HOMO leads to the population of the tightly bound $X^2\sum^+$ ground state of the molecular cation, mostly forming the nondissociative molecular ion CO^+. The $A^2\Pi$ or $B^2\sum^+$ excited states are populated by removing a HOMO-1 or HOMO-2 electron, respectively, which are afterwards photon coupled to dissociative states and break into the C^+ and O fragments [38,39]. These dynamics are encoded in the orbital and vibrational resolved electron-nuclear JES. For a given dissociation pathway, by considering the aforementioned two-step model, the observed discrete E_N peaks map the energy spacing of the adjacent vibrational levels from which the dissociation is initialized. As shown in Fig. 1(b), two adjacent E_N peaks are separated by about 0.17 eV for both the low-E_N and high-E_N regions, which matches well with the vibrational energy spacing of the excited $A^2\Pi$ ($\delta E_v \sim 0.17$ eV for $v = 1$–4) or $B^2\sum^+$ ($\delta E_v \sim 0.16$ eV for $v = 8$–12) states but mismatches with the ground $X^2\sum^+$ state ($\delta E_v \sim 0.20$ eV to 0.27 eV for $v = 0$–20). By excluding the $X^2\sum^+$ state, as illustrated in Fig. 2(a), the high- and low-E_N regions are most likely produced in the following approaches: An ionization created vibrational nuclear wave packet on the $A^2\Pi$ state is two-photon coupled to the $D^2\Pi$ state and dissociates to the $C^+(^2P^0) + O(^3P)$ limit, leading to the observed events with $E_N > 0.7$ eV in the high-E_N region, while the observed events with $E_N < 0.7$ eV can be attributed to the one-photon transition of the nuclear wave packet from the $B^2\sum^+$ state to the $3^2\sum^+$ and $3^2\Pi^+$ states, followed by dissociation to the $C^+(^2P^0) + O(^1D)$ limit. The locations of the expected E_N of the one- and two-photon dissociation from various vibrational levels in the $A^2\Pi$ ($v = 4$ to 1) and $B^2\sum^+$ ($v = 12$ to 8) states are marked (dashed lines) in the top panel of Fig. 2(b), respectively, which are in good agreement with the measurements.

Since electrons from different orbitals are released, the momentum distribution of the emitted photoelectron correlated with the C^+ in the low-E_N region is noticeably different from that correlated with the C^+ in the high-E_N region, as shown in Figs. 3(a) and 3(b), respectively. In addition, as displayed in Figs. 3(c) and 3(d), the emitted C^+ also have different angular distributions for two different dissociative ionization pathways.

To further verify that the observed fine structures in the E_N spectrum map the vibrational states of the CO^+ from which the dissociation is initialized, we numerically simulate the dissociation process by solving the modeled time-dependent Schrödinger equation [atomic units (a.u.) are used throughout unless indicated otherwise]

$$i\frac{\partial}{\partial t}\begin{pmatrix}\chi_1(R,t)\\ \chi_2(R,t)\\ \chi_3(R,t)\\ \vdots\end{pmatrix} = \begin{pmatrix} T+V_1(R) & \overrightarrow{\mu_{12}}\cdot\overrightarrow{E(t)} & \overrightarrow{\mu_{13}}\cdot\overrightarrow{E(t)} & \cdots \\ \overrightarrow{\mu_{12}}\cdot\overrightarrow{E(t)} & T+V_2(R) & \overrightarrow{\mu_{23}}\cdot\overrightarrow{E(t)} & \cdots \\ \overrightarrow{\mu_{13}}\cdot\overrightarrow{E(t)} & \overrightarrow{\mu_{23}}\cdot\overrightarrow{E(t)} & T+V_3(R) & \cdots \\ \vdots & \vdots & \vdots & \ddots \end{pmatrix} \times \begin{pmatrix}\chi_1(R,t)\\ \chi_2(R,t)\\ \chi_3(R,t)\\ \vdots\end{pmatrix} \quad (1)$$

in which the six electronic states of CO^+ shown in Fig. 2(a) are included. χ_1 to χ_3 and χ_4 to χ_6 are the associated nuclear wave packets for the three Σ states and three Π states from bottom to top, respectively. T is the nuclear kinetic energy

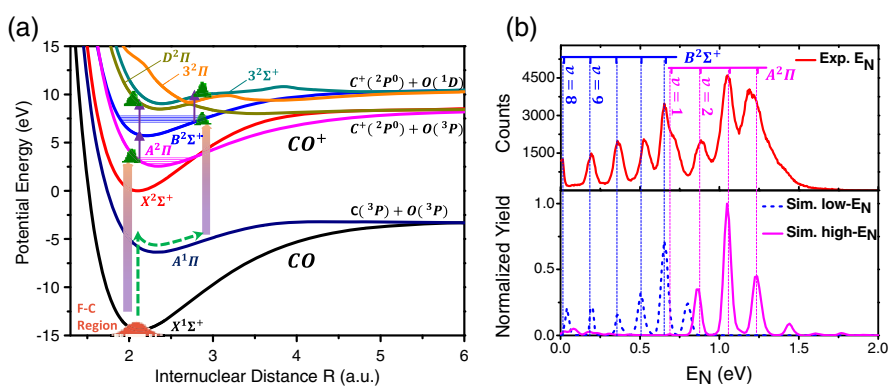

FIG. 2. (a) Relevant potential energy surfaces of CO and CO^+. (b) Measured (top panel) and simulated (bottom panel) nuclear kinetic energy spectra E_N. The locations of the excepted E_N of one- and two-photon absorption from different vibrational levels in $B^2\sum^+$ and $A^2\Pi$ states are marked in the top panel.

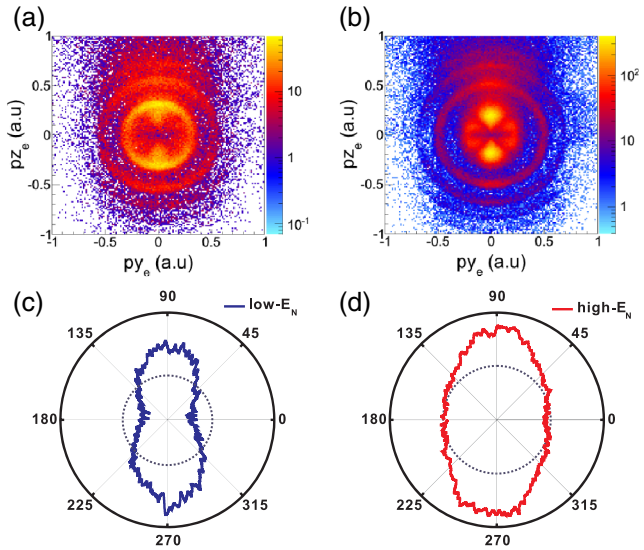

FIG. 3. Measured (a),(b) momentum distributions of the emitted electrons and (c),(d) angular distributions of the ejected C^+ of the $CO(1,0)$ channel in the (a),(c) low-E_N and (b),(d) high-E_N regions.

operator, and the R-dependent dipole coupling matrix elements μ_{ij} $(1 \le i \le 6,\ 1 \le j \le 6,\ i \ne j)$ are calculated by the molpro [36]. The laser pulse $E(t)$ is the same as that used in the experiment. The time and spatial steps are $\delta t = 0.1$ a.u. and $\delta R = 0.02$ a.u. The simulation box is big enough to hold all wave packets. The kinetic energy of the nuclei is obtained using the windows operator [40] after the interaction of the laser pulse.

In calculations, we first launched the Frank-Condon nuclear wave packet onto the $X^2\sum^+$, $A^2\Pi$, or $B^2\sum^+$ states. We found the dissociation starting from $A^2\Pi$ dominates other channels after considering the probabilities of the single ionization of CO and later dissociation probabilities of CO^+. The calculated E_N is shown by the pink solid curve in Fig. 2(b), which agrees with the measured high-E_N spectrum. Alternatively, CO may absorb three photons and populate the $A^1\Pi$ state of CO, which will relax to a larger internuclear distance, from where an electron is removed and the nuclear wave packet is projected onto $B^2\sum^+$, which will afterward be coupled into dissociative states such as $3^2\sum^+$ or $3^2\Pi$ in the remaining laser field. In simulations, we thus put the Frank-Condon nuclear wave packet on $A^1\Pi$, which will relax to the outer turning point after around 30 fs. Then, the nuclear wave packet at the outer turning point is further projected onto $B^2\sum^+$, whose later fate is governed by Eq. (1). This reaction pathway finally contributes the low E_N, as shown by the dashed blue curve in Fig. 2(b). The nice agreement between calculations and measurements shown in Fig. 2(b) confirms our explanation. Only if the pulse duration is much larger than the vibrational period, the discrete E_N can be readily distinguished by resolving the vibrational dynamics. For the involved vibrational states of $A^2\Pi$ and $B^2\sum^+$ with vibrational periods of ~22 and ~25 fs, respectively, we estimate that a laser pulse with a duration longer than 30 fs is needed to resolve the vibrational structure in the observed E_N spectra.

By tracing different dissociative ionization pathways, one may retrieve how the slopes change when multiple orbitals and electronic states are involved. Assuming the single ionization of CO occurs at a certain internuclear distance R_1, and the coupling between different electronic states [with the corresponding Born-Oppenheimer potential curves $V_2(R)$ and $V_3(R)$] at a certain R_2 triggers the dissociation of CO^+, one may derive $E_N(R_1,R_2) + E_e(R_1) \sim \Delta V(R_2) - U_p(R_1)$, where $\Delta V(R_2) = V_3(R_2) - V_2(R_2)$ and $U_p(R_1)$ is the ponderomotive energy. Note that here V_2 and V_3 are just some general potential curves. The independence of ΔV and U_p on the internuclear distance should give a slope of -1. However, for instance, with the low and high E_N in the dissociation of CO^+, ΔV corresponds to the energy difference of $3^2\sum^+$-$B^2\sum^+$ and $D^2\Pi$-$A^2\Pi$, respectively, and both ΔV decrease with the increasing of the internuclear distance. Furthermore, the former decreases more rapidly than the latter. Thus, the slope in the low E_N is smaller than that in the high E_N. This qualitatively explains the different slopes in the electron-nuclear JES spectrum of the $CO(1,0)$ channel for different dissociation pathways. A quantitative reproduction of the slope requires a precise description of the complex ionization dynamics of the multielectron molecule, which is beyond our current numerical model.

As compared to the $H_2{}^+$ [20–27] and H_2 [28], the JES for the dissociative ionization of CO shows several common and different characters. First of all, JES is a general process in the dissociative ionization of molecules, which is a strong proof of electron-nuclei coupling in ultrafast chemical reactions. Freeman resonance is present in the JES for both H_2 and CO [indicated by the red arrow in Fig. 1(a)] only when linearly polarized laser fields are used. However, because of the complexity of the multielectron system, the JES for the dissociative ionization of CO has more structures: the vibrational structures are more distinct, and the low- and high-E_N regions have different slopes, as shown in Fig. 1(d). Different slopes of the JES actually indicate the participation of multiple orbitals and electronic states in the strong-field dissociative single ionization of the multielectron molecule. As compared to a pioneering experiment [28], we did resolve the vibrational structure of $H_2{}^+$ in our recent measurement with refined experimental conditions. The visibility of the vibrational structure in the spectra depends not only on the ratio of the vibrational periods to the temporal duration of the laser pulse, but also the detailed experimental conditions such as the intensity and focusing condition of the laser field and the energy resolution of the spectrometer.

In summary, by measuring the fragment ion and electron ejected from a singly ionized CO in coincidence, we experimentally demonstrate the correlated electron-nuclear sharing of the excess photon energy in above-threshold multiphoton ionization of multielectron molecules. The

vibrational energy reservoir, i.e., population of numerous vibrational states in the ionization process, plays an important role in the electron-nuclear sharing of the absorbed photon energy. Differing from the simplest one- or two-electron molecules, the participation of various orbitals and the coupling of various electronic states of the multielectron molecule alter the observed electron-nuclear sharing of the absorbed photon energy. Our results provide deep insight into the correlated electron-nuclear dynamics of multielectron molecules in strong-field ionization processes, in particular, the photon energy deposition as the primary stage of the light-molecule interaction.

We thank Y. Liu for our helpful discussion. This work is supported by the National Natural Science Fund (Grants No. 11425416, No. 11374103, No. 11434005, No. 11322438, and No. 11574205). Program of Introducing Talents of Discipline to Universities (Grant No. B12024).

*fhe@sjtu.edu.cn
†hpzeng@phy.ecnu.edu.cn
‡jwu@phy.ecnu.edu.cn

[1] P. H. Bucksbaum, A. Zavriyev, H. G. Muller, and D. W. Schumacher, Phys. Rev. Lett. **64**, 1883 (1990).
[2] M. Magrakvelidze, F. He, T. Niederhausen, I. V. Litvinyuk, and U. Thumm, Phys. Rev. A **79**, 033410 (2009).
[3] L. J. Frasinski, J. H. Posthumus, J. Plumridge, K. Codling, P. F. Taday, and A. J. Langley, Phys. Rev. Lett. **83**, 3625 (1999).
[4] G. Yao and Shih-I Chu, Phys. Rev. A **48**, 485 (1993).
[5] A. Giusti-Suzor, X. He, O. Atabek, and F. H. Mies, Phys. Rev. Lett. **64**, 515 (1990).
[6] G. Jolicard and O. Atabek, Phys. Rev. A **46**, 5845 (1992).
[7] Z. C. Li, C. Ruiz, and F. He, Phys. Rev. A **90**, 033421 (2014).
[8] H. Stapelfeldt, E. Constant, and P. B. Corkum, Phys. Rev. Lett. **74**, 3780 (1995).
[9] B. D. Esry, A. M. Sayler, P. Q. Wang, K. D. Carnes, and I. Ben-Itzhak, Phys. Rev. Lett. **97**, 013003 (2006).
[10] A. Hishikawa, A. Iwamae, K. Hoshina, M. Kono, and K. Yamanouchi, Chem. Phys. **231**, 315 (1998).
[11] T. Zuo and A. D. Bandrauk, Phys. Rev. A **52**, R2511 (1995).
[12] S. Chelkowski, A. D. Bandrauk, A. Staudte, and P. B. Corkum, Phys. Rev. A **76**, 013405 (2007).
[13] M. Ferray, A. L' Huillier, X. F. Li, L. A. Lompré, G. Mainfray, and C. Manus, J. Phys. B **21**, L31 (1988).
[14] J. L. Krause, K. J. Schafer, and K. C. Kulander, Phys. Rev. Lett. **68**, 3535 (1992).
[15] A. L'Huillier, M. Lewenstein, P. Salières, Ph. Balcou, M. Yu. Ivanov, J. Larsson, and C. G. Wahlstrom, Phys. Rev. A **48**, R3433 (1993).
[16] A. Lafosse, M. Lebech, J. C. Brenot, P. M. Guyon, O. Jagutzki, L. Spielberger, M. Vervloet, J. C. Houver, and D. Dowek, Phys. Rev. Lett. **84**, 5987 (2000).
[17] F. Martín, J. Fernández, T. Havermeier, L. Foucar, Th. Weber, K. Kreidi, M. Schöffler, L. Schmidt, T. Jahnke, O. Jagutzki, A. Czasch, E. P. Benis, T. Osipov, A. L. Landers, A. Belkacem, M. H. Prior, H. Schmidt-Böcking, C. L. Cocke, and R. Dörner, Science **315**, 629 (2007).
[18] T. Osipov, T. N. Rescigno, T. Weber, S. Miyabe, T. Jahnke, A. S. Alnaser, M. P. Hertlein, O. Jagutzki, L. Ph. H. Schmidt, M. Schöffler, L. Foucar, S. Schössler, T. Havermeier, M. Odenweller, S. Voss, B. Feinberg, A. L. Landers, M. H. Prior, R. Dörner, C. L. Cocke, and A. Belkacem, J. Phys. B **41**, 091001 (2008).
[19] P. Agostini, F. Fabre, G. Mainfray, G. Petite, and N. K. Rahman, Phys. Rev. Lett. **42**, 1127 (1979).
[20] C. B. Madsen, F. Anis, L. B. Madsen, and B. D. Esry, Phys. Rev. Lett. **109**, 163003 (2012).
[21] R. E. F. Silva, F. Catoire, P. Rivière, H. Bachau, and F. Martín, Phys. Rev. Lett. **110**, 113001 (2013).
[22] L. Yue and L. B. Madsen, Phys. Rev. A **88**, 063420 (2013).
[23] K. L. Liu, P. F. Lan, C. Huang, Q. B. Zhang, and P. X. Lu, Phys. Rev. A **89**, 053423 (2014).
[24] F. Catoire, R. E. F. Silva, P. Rivière, H. Bachau, and F. Martín, Phys. Rev. A **89**, 023415 (2014).
[25] V. Mosert and D. Bauer, Phys. Rev. A **92**, 043414 (2015).
[26] Z. Wang, M. Li, Y. Zhou, Y. Li, P. Lan, and P. Lu, Phys. Rev. A **93**, 013418 (2016).
[27] L. Yue and L. B. Madsen, Phys. Rev. A **93**, 031401 (2016).
[28] J. Wu, M. Kunitski, M. Pitzer, F. Trinter, L. Ph. H. Schmidt, T. Jahnke, M. Magrakvelidze, C. B. Madsen, L. B. Madsen, U. Thumm, and R. Dörner, Phys. Rev. Lett. **111**, 023002 (2013).
[29] X. Gong, Q. Song, Q. Ji, K. Lin, H. Pan, J. Ding, H. Zeng, and J. Wu, Phys. Rev. Lett. **114**, 163001 (2015).
[30] R. Dörner, V. Mergel, O. Jagutzki, L. Spielberger, J. Ullrich, R. Moshammer, and H. Schmidt-Böcking, Phys. Rep. **330**, 95 (2000).
[31] J. Ullrich, R. Moshammer, A. Dorn, R. Dörner, L. P. H. Schmidt, and H. Schmidt-Böcking, Rep. Prog. Phys. **66**, 1463 (2003).
[32] O. Jagutzki, A. Cerezo, A. Czasch, R. Dörner, M. Hattaß, M. Huang, V. Mergel, U. Spillmann, K. Ullmann-Pfleger, T. Weber, H. Schmidt-Böcking, and G. D. W. Smith, IEEE Trans. Nucl. Sci. **49**, 2477 (2002).
[33] K. Henrichs, M. Waitz, F. Trinter, H. Kim, A. Menssen, H. Gassert, H. Sann, T. Jahnke, J. Wu, M. Pitzer, M. Richter, M. S. Schöffler, M. Kunitski, and R. Dörner, Phys. Rev. Lett. **111**, 113003 (2013).
[34] J. Wu, L. Ph. H. Schmidt, M. Kunitski, M. Meckel, S. Voss, H. Sann, H. Kim, T. Jahnke, A. Czasch, and R. Dörner, Phys. Rev. Lett. **108**, 183001 (2012).
[35] H. Akagi, T. Otobe, A. Staudte, A. Shiner, F. Turner, R. Dörner, D. M. Villeneuve, and P. B. Corkum, Science **325**, 1364 (2009).
[36] H.-J. Werner, P. J. Knowles *et al.*, MOLPRO, version 2015.1, 2015.
[37] K. Okada and S. Iwata, J. Chem. Phys. **112**, 1804 (2000).
[38] I. Znakovskaya, P. von den Hoff, S. Zherebtsov, A. Wirth, O. Herrwerth, M. J. J. Vrakking, R. de Vivie-Riedle, and M. F. Kling, Phys. Rev. Lett. **103**, 103002 (2009).
[39] S. De, M. Magrakvelidze, I. A. Bocharova, D. Ray, W. Cao, I. Znakovskaya, H. Li, Z. Wang, G. Laurent, U. Thumm, M. F. Kling, I. V. Litvinyuk, I. Ben-Itzhak, and C. L. Cocke, Phys. Rev. A **84**, 043410 (2011).
[40] K. J. Schafer and K. C. Kulander, Phys. Rev. A **42**, 5794 (1990).